
Article:
Nichols, A., Tait, S., Horoshenkov, K. et al. (2013) A Non-invasive wave monitor. Flow Measurement and Instrumentation, 34. pp. 118-126. ISSN: 0955-5986

https://doi.org/10.1016/j.flowmeasinst.2013.09.006

An non-invasive airborne wave monitor

A.Nichols[1], S. Tait[1], K. Horoshenkov[1], and S. Shepherd[1]
[1]School of Engineering, Design & Technology
University of Bradford
Bradford, West Yorkshire
UNITED KINGDOM
E-mail: a.nichols2@bradford.ac.uk

Abstract: *This work presents a new acoustic method for remote measurement of the surface characteristics of the dynamic air-water interface in free-surface flows. The technique uses acoustic reflection of a monochromatic ultrasonic wave by the dynamically rough air-water interface to measure relative water surface position. It is found that with careful selection of the acoustic components and their configuration, the phase of the reflected signal responds to the local fluctuations in the fluid interface at the point of specular acoustic reflection. In order for the method to be applicable, three criteria must be satisfied: (1) The dominant wavelength of the surface under investigation must be greater than the first Fresnel zone of the acoustic system; (2) The mean magnitude of the instantaneous local surface gradient must not exceed 0.025; (3) The RMS wave height must be greater than 1% of the acoustic wavelength. Under these conditions the mean error of the system is within 5.4% of the acoustic wavelength, and usually within 1%, while the error relative to the largest wave heights does not exceed 4%. This error may be reduced by properly tuning the acoustic wavelength to the surface of interest. For turbulent flows, the surface waves fall well within the criteria, and the absolute errors are independent of wave height, so for larger wave heights, the relative error can be considerably low. The technique provides a robust system for monitoring the dynamics of free surface flows, which is non-invasive, low cost, and low power. The method is applied to laboratory flows but has greater potential in remote sensing of free surface properties on a local scale in field environments where invasive techniques are difficult to implement. It is therefore of considerable potential application to the fields of oceanography, hydrology, and water resources.*

Keywords: *Remote sensing, Water surface, Environment, Ultrasonic, Phase, Monitoring.*

1. INTRODUCTION

Wave monitors give a measure of the level of fluid at a point or small area. This type of measurement is useful in a number of areas. In hydraulic research, various forms of wave monitor are commonly used to measure the interface characteristics generated by various flow regimes (Nichols et al, 2010; Denissenko et al, 2008) and hydraulic phenomena (Wilde et al, 1998). They are used in scale modelling to estimate the effect of geometric changes on the flow depth or wave height (Bullocka et al, 2007) at given points in a flow system and in some field investigations to measure the wave properties of rivers, estuaries and oceans (Barjenbruch et al, 2002).

Various forms of wave monitor exist. The vast majority are invasive in nature, meaning they must be inserted into the fluid in order to function. The most common invasive wave probes are electrical in nature, and function either through conductance or capacitance. Conductance type wave probes consist of two parallel elongate electrodes separated by a small distance. These conductors are normally oriented vertically through the flow surface. An alternating (usually square-wave) current is passed between the two electrodes, and the conductance is recorded. Any change in the local free-surface level causes a change in the submergence of the two electrodes. This effects a proportional change in the conductance. A calibration is recorded which describes the (usually) linear relationship between conductance and submergence, and this calibration is then applied to experimental data in order to output a time series of submergence or flow depth. The accuracy is determined by the data acquisition device and the residual electrical noise level, while the temporal resolution of data is limited by the data acquisition device and the frequency of the AC excitation current. The spatial accuracy is limited by the separation of the two electrodes, and the spatial resolution of multiple measurements is determined by the separation of adjacent probes. This is limited by the need to avoid excessive

interaction between the electrical signals of multiple probes, a phenomenon which can be mitigated to some extent by using a different excitation frequency for each probe.

Capacitance type probes are similar to conductance type since they too involve the device penetrating the flow surface. A rod is used to keep an insulated wire taught and vertical. The rod serves as a zero potential electrode. The insulated wire is then operated as a capacitor, whereby the wire forms one plate of a coaxial capacitor, the water forms the other plate, and the insulation forms the dielectric medium in between. As the water level rises and falls, the effective common length of the capacitor plates changes proportionally and generates a proportional change in the capacitance measured between the insulated wire and the zero-potential rod. This technique provides a more accurate spatial measurement, since the fluctuations are quantified at the small point at which the insulated wire penetrates the surface. Again a calibration is required, and the accuracy is determined by the residual electrical noise level, while the temporal resolution of data is limited by the data acquisition device and the frequency of excitation.

Both of these electrical techniques suffer from two inherent disadvantages. Firstly, the data may only be trusted while the conditions under which the calibration was obtained are upheld. Any variation in the electrical properties of the fluid, for example to due change in the ambient temperature of the fluid, will invalidate the readings. For this reason these types of devices are most commonly used only under well controlled conditions.

Secondly, they must penetrate the flow surface in order to obtain a reading. There are many scenarios where this type of invasive technology is impractical, most notably when flows contain solids or suspended particles. These materials in the flow accumulate on the instrument and cause the loss of calibration so that the data become invalid. Wastewater flows are a good example of this. Furthermore, in some situations the probes themselves may generate capillary waves of sufficient magnitude to corrupt the surface pattern. In the experiments reported here the probes were sufficiently thin, and the flows sufficiently slow, so that this was not the case.

A number of attempts have been made to quantify local surface fluctuations optically. Some research has investigated the use of infra-red and laser displacement techniques (Daida et al. (1995); Takamasa & Hazuku, 2000), however this is difficult to implement for real flows since water surfaces are poor reflectors of light (most of the energy passes through the surface). Some work has also been conducted using stereoscopic imaging to monitor the vertical location of one or more specific points on a water surface (Tsubaki & Fujita, 2005). This has a high degree of accuracy, and is totally non-invasive, however the surface must be marked in fixed locations, usually by laser or by projector. In order for the markings to be clear and comparable between the two camera images, the water surface must again reflect the light well. This is usually achieved by adding a colorant to the water, but this is not practical for most fluvial or wastewater flows. These techniques also require a calibration to take place, which is impractical for many applications, and has the potential to change undetectably over time.

Clearly there is a need for a technology capable of measuring local water surface fluctuations which is less invasive than electrically based techniques and more robust for field or real-world applications than optical methods. One attractive option is the use of acoustic instrumentation, since water surfaces are acoustically hard and therefore reflect acoustic signals well.

Acoustic techniques are well studied in the context of range finding, and for monitoring the average location of fluid interfaces. The simplest and most commonly used technique is a basic time-of-flight (TOF) measurement, whereby an acoustic pulse is emitted, reflects back from an area of a surface, and the time between emission and reception of the reflection indicates the average distance to the surface (based on an assumed or independently measured local sound speed). A recent example of this kind of technology is described by Lagergren et al (2012). Some technologies project acoustic energy toward the surface and then analyse the phase of the received signal in order to estimate an absolute value of the mean fluid surface level (Redding, 1983). Wang et al (1991) used phase measurements to monitor the overall depth, rather than local fluctuations in a fluid of constant depth, and so no consideration was given to the effect of the surface pattern on the output of the system. Delafon (1975) used a similar technique to monitor level changes. This work required an acoustic waveguide in the form of a pipe to be placed into the fluid to direct the acoustic field to and from the

surface. The use of a penetrating physical wave guide would of course disrupt the flow and affect strongly the fluctuating water surface pattern.

Whilst these techniques provide a measure of the mean surface position, they do not allow the detection of local surface fluctuations at a point or small area. The purpose of this work is to quantify local free surface fluctuations and to ascertain the surface parameters necessary for such a technique to be viable.

There is some precedent for using acoustic techniques to characterise relatively small-scale roughness, but these rough surfaces have historically been static in nature, unlike the dynamic roughness of turbulent flow surfaces. Oelze (2003) for example has examined the use of acoustic backscatter to measure soil surfaces, whilst Attenborough et al (1995) and Nichols et al (2011) have built on the work of Tolstoy (1984) to develop methods of characterising static surfaces by measurement of excess attenuation spectra of a forward-scattered signal. Cooper et al (2006) investigated the link between the statistical properties of a spherical audio pulse propagating over a flow surface and the hydraulic properties of the flow. A link was discovered between the second moment of acoustic intensity and the hydraulic roughness coefficient of the flow. The only explanation for this relationship is the rough water interface, which links the two phases, having a measurable effect on the audio signal; however this relationship was not investigated.

This work investigates a method of measuring the dynamic fluctuations of a water surface by analysis of the temporal variation of a reflected acoustic wave. Whereas Cooper et al (2006) used a series of spherical audio pulses; this work uses a continuous monochromatic ultrasonic wave. This allows direct analysis of the time series, rather than statistical analysis of discrete measurements. The ultrasonic transducer also provides a more directional acoustic signal, minimising unwanted multiple reflections, and approximating closer to measuring a point on the surface rather than an area.

2. ACOUSTIC THEORY

An incident acoustic plane wave $v_s(t) = A_0 e^{i\omega_s t}$ is reflected from an acoustically hard surface and the reflected acoustic wave $v_r(t) = A_r e^{i\omega_s t + i\varphi_s}$ which is received at a microphone some distance away has a difference in phase, φ_s, when compared to the transmitted signal, due to the time taken for the acoustic wave to travel from source to receiver. Here ω_s is the signal frequency, A_0 is the amplitude of the incident sound wave, A_r is the amplitude in the reflected sound wave, t is the time and $i = \sqrt{-1}$. When the reflecting boundary is stationary the phase difference φ_s is constant and time independent. If the surface moves vertically, then the phase difference and the amplitude in the reflected wave can be altered due to the change in path-length and the boundary roughness as shown in Figure 1.

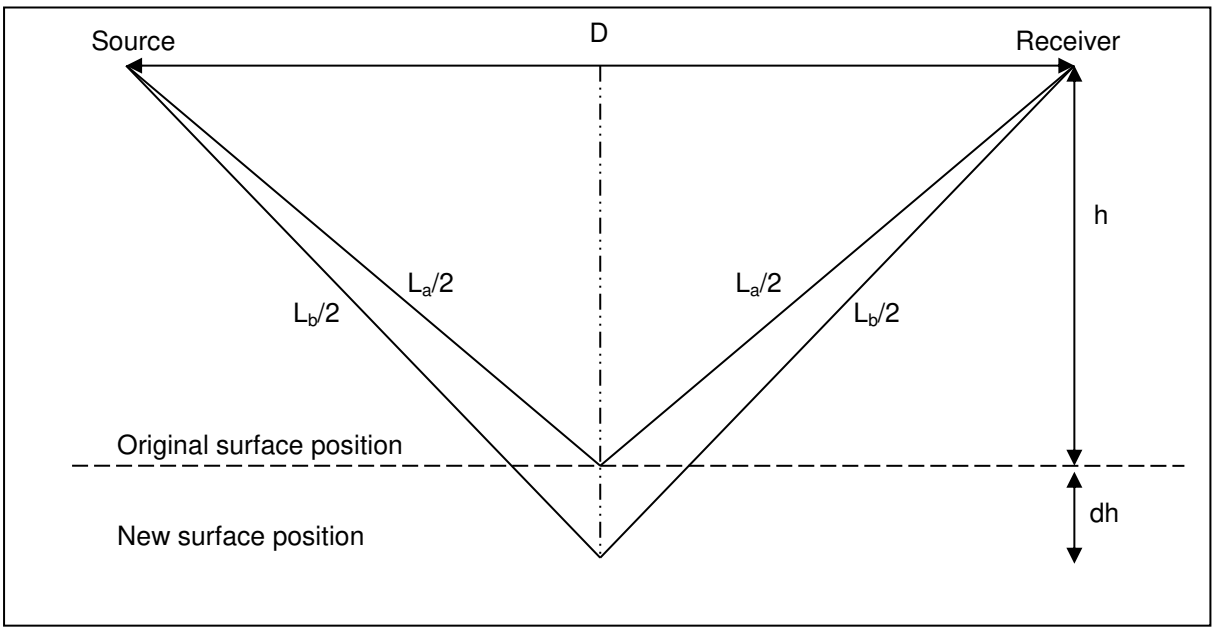

Figure 1: Change in effective path-length caused by surface movement

Here the source and receiver are both a distance 'h' above the mean position of the water surface, separated by a distance 'D'. The change in phase difference caused by the surface moving down by a distance of 'Δh' is given by:

$$\Delta\varphi(t) = -2\pi\Delta L(t)/\lambda. \qquad (1)$$

Here λ is the acoustic wavelength and $\Delta L(t)$ is the time-dependent change in path-length given by:

$$\Delta L = L_b - L_a, \qquad (2)$$

where L_a and L_b are the original and new path-lengths respectively, given by:

$$L_a = 2\sqrt{\left(\frac{D}{2}\right)^2 + h^2} \qquad L_b = 2\sqrt{\left(\frac{D}{2}\right)^2 + (h+\Delta h)^2}. \qquad (3)$$

In expressions (2) and (3) we omit the time dependence for brevity. Reversing the process, the change in surface position, *Δh*, can be calculated directly from the recorded variation in phase difference:

$$\Delta h = \sqrt{\left(\frac{L_b}{2}\right)^2 - \left(\frac{D}{2}\right)^2} - h \qquad \text{where} \quad L_b = \Delta L + L_a \quad \text{and} \quad \Delta L = -\Delta\varphi\lambda/2\pi. \qquad (4)$$

In order for the surface fluctuations to be measured, the phase difference between the transmitted and recieved time series must be determined. A relatively straightforward method to determine the phase is to use the well-known relations from the analytic signal theory, i.e.:

$$\frac{v_r(t)}{v_s(t)} = \frac{A_r(t)}{A_0} e^{i(\varphi_s + \Delta\varphi(t))}, \qquad (5)$$

from which

$$\varphi(t) = \varphi_s + \Delta\varphi(t) = \mathrm{Im}\left\{\log\left(\frac{v_r(t)}{v_s(t)}\right)\right\}. \qquad (6)$$

In expression (6) the time dependent term $\Delta\varphi(t)$ is of practical interest. The constant phase term in expression (6) can be determined either as the phase of the reflected acoustic wave at $t = 0$ or in the case of the fluctuating water level as the mean phase, i.e. $\varphi_s = \langle\varphi(t)\rangle$.

The spatial accuracy of this technique is limited by the 'footprint' of the acoustic signal, i.e. by the illuminated area of the fluctuating water surface which contributes to the sound field at the receiver point. This may be estimated by the Fresnel theory (e.g. Nocke (2000)), which enables to define a zone on the reflecting surface for which the distance from source to receiver, via any point in that zome, does not exceed the distance of the specular reflection by more than a predetermined value, F. This value of the path length difference is usually expressed in multiples of the wavelength λ. For acoustically hard surfaces, such as water, two adjacent Fresnel zones defined by F=n/2 with n=1,2,3,… will cancel as their contributions to the total field are out of phase. This has been proven experimentally by Spandöck (1934) for acoustic waves. Furthermore, as the amplitude excited by following Fresnel zones decreases, the first (half) zone makes the most important contribution to the

total field, e.g. F=1/2. Assuming that all areas of this dominant Fresnel zone contribute equally to the received signal, this would mean the technique would be suitable for measuring waves with a spatial period greater than the Fresnel zone diameter. This forms the first criterion for the assessment of the area of Fresnel zone. In reality, transducers have a directivity pattern which generates greater energy levels in the specular direction. Therefore, the effective Fresnel zone is generally smaller than predicted by the Fresnel theory and depends on the transducer directivity.

3. EXPERIMENTAL SETUP

It has been shown above that fluctuations in water surface position may be quantified by measurement of the variation in the phase difference between a sent and received signal reflected from a dynamic air-water interface. To demonstrate this, acoustic data was compared to water surface data recorded by wave probes in a 12m long, 0.46m wide tilting flume. The substrate used in the flume was river gravel with a near normal distribution about a mean grain size of 4.5mm, and standard deviation 1.7mm. The bed was scraped flat with no appreciable bedforms. First, the flume was set to a horizontal gradient and simple gravity waves with large spatial scale were generated in still water. Then the flume was tilted to a gradient of 0.004 and a range of steady flows were established in order to generate surface fluctuations of varying scale and spectral composition. Flow conditions were selected to ensure a non-mobile bed. These flows were sub-critical and a downstream control was adjusted so as to ensure uniform flow conditions at the measurement location.

3.1. Acoustic setup

The acoustic system was located 9m from the upstream end of the flume. An ultrasonic transducer (ceramic type 043SR750) with the main resonance frequency of 45kHz was positioned at an angle of 45° to the mean water surface position, at a distance of 0.4m from the point of incidence. A single Brüel & Kjær (B&K) ¼" type 4930 microphone was placed in the path of the specular reflection, also at a distance of 0.4m from the incident point as shown in Figure 2. The transducer was excited at its resonant frequency in order to produce a continuous sine wave.

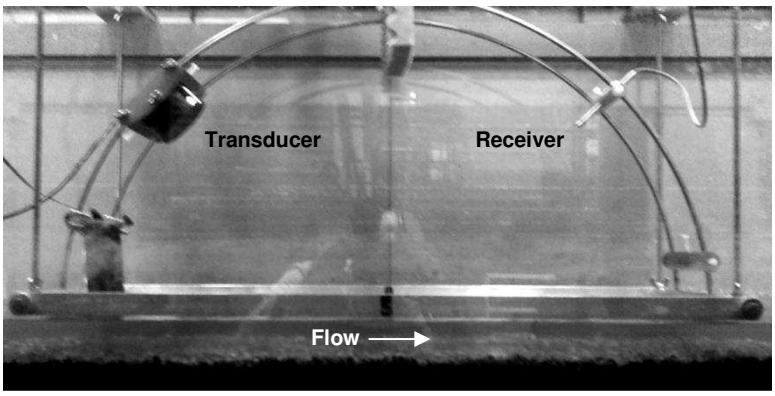

Figure 2: Instrument set up

3.2. Wave probe setup

In order to quantify the performance of the acoustic based instrumentation the water surface elevation at the point of specular reflection was recorded using a Churchill twin-wire conductant wave probe. The thickness of the wires in the wave probe was 0.25 mm, which is sufficiently smaller than the acoustic wavelength to cause any additional scattering. By energising the two partially submerged wires, the probe gave a voltage output proportional to the amount of probe that was below the water surface. By applying a predetermined calibration, the probe directly output the instantaneous depth of the water against time.

3.3. Data acquisition & signal processing

A National Instruments LabView data acquisition system was used to record the acoustic signal at 1 MHz sampling rate. The wave probe data was collected at the sampling rate of 10kHz. The data acquisition was carried out in 1 ms packets to avoid memory overflow. . These packets of ddata were recorded synchronously, and the acquisition of each packet was triggered at a rate of 45Hz.

Each acoustic packet was analysed according eq. (6) so that the mean of the time-dependent phase difference was calculated for each packet. The phase time series obtained from this analysis was then unwrapped in order to correct for the phase switching between + π and - π when the change in surface elevation exceeded one acoustic wavelength (i.e. $\Delta L > \lambda = 7.6$ mm). The process described by eq. (4) was then used to convert phase difference values into surface elevation measurements so that the water surface elevation could be presented as a function of time. Each packet of wave probe data was averaged to remove high frequency noise, resulting in a wave probe time series sampled at 45Hz. A 3rd order 10 Hz low-pass Butterworth filter was then applied to the surface elevation data from the wave probes and the acoustically derived measurements. This threshold was selected since the Churchill wave monitor includes an internal 10 Hz low-pass filter, so any signal above this threshold was assumed to be due to noise. The wave probe data was then used to validate the results of acoustically based measurements.

4. GRAVITY WAVES

In the first stage of testing, the flume was set at a gradient of zero with its upstream and downstream ends sealed so that still water conditions were simulated. Simple pseudo-sinusoidal surface gravity waves were generated by manually oscillating a plate at one end of the flume which was hinged at the bed as shown in Figure 3. These waves were generated at four different water depths: 86mm, 119mm, 158mm and 181mm. At each depth the excitation plate was manually operated at three approximate frequencies of 0.5Hz, 1Hz, and 2Hz. For each frequency at each depth, the angular range of motion of the excitation plate was manually controlled to approximately ±5°, ±10°, and ±20° from vertical. This resulted in thirty-six individual wave regimes, each with different wave properties (frequency, wavelength, wave height, phase speed).

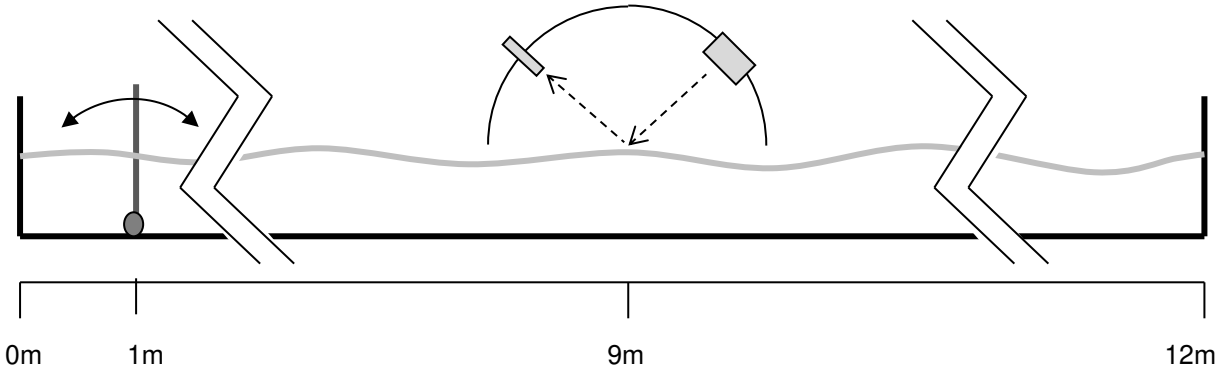

Figure 3: Simple surface wave excitation

For each of the thirty-six regimes, surface elevation data was recorded synchronously by the wave probe and the acoustic device. A time window was applied so as to eliminate any waves reflected from the end of the flume. The wave probe data was used to quantify the mean depth, *d*, and the root-mean-square (RMS) wave height, h_{rms}). The dominant frequency component, *f*, was also calculated by taking a weighted average of the frequency spectrum, whereby the frequency components were weighted by their Fourier coefficient. Using the measured depth and frequency, a least squares minimisation routine determined the phase speed, Cp, by finding the optimum value to minimize variable *z* in eq. (7) , which is based on linear wave theory for gravity wave propagation (Airy, 1841).

$$z = C_p - \sqrt{\frac{gC_p}{2\pi f} tanh\left(\frac{2\pi f d}{C_p}\right)}. \quad (7)$$

Once the dominant frequency and phase speed were known, it was possible to calculate the dominant wavelength, $\lambda = Cp/f$. These data are given in Table 1.

Table 1: Gravity wave regimes (wave probe data)

Wave regime	Average depth d (m)	Fluctuation frequency f (Hz)	Phase speed Cp (m/s)	Wavelength λ (m)	RMS wave height h_{rms} (mm)
1	0.086	1.0	0.86	0.85	0.04
2	0.086	0.8	0.88	1.07	0.11
3	0.086	0.7	0.89	1.22	0.21
4	0.085	1.5	0.79	0.51	0.02
5	0.085	1.2	0.84	0.71	0.05
6	0.085	1.1	0.85	0.77	0.15
7	0.085	2.0	0.71	0.36	0.02
8	0.085	1.4	0.81	0.56	0.03
9	0.085	1.1	0.85	0.78	0.08
10	0.119	1.1	0.99	0.94	0.47
11	0.119	0.7	1.00	1.34	0.98
12	0.119	0.9	1.00	1.13	1.23
13	0.119	1.4	0.91	0.65	0.56
14	0.119	1.2	0.96	0.82	1.04
15	0.119	0.9	1.00	1.08	2.06
16	0.119	2.2	0.69	0.31	0.36
17	0.119	2.0	0.75	0.38	1.68
18	0.118	1.6	0.86	0.54	1.88
19	0.158	1.0	1.00	1.00	2.04
20	0.158	0.7	1.00	1.36	3.60
21	0.158	0.9	1.00	1.09	4.06
22	0.158	2.0	0.77	0.38	4.58
23	0.158	1.5	0.94	0.61	6.20
24	0.158	1.3	1.00	0.77	9.78
25	0.158	2.1	0.75	0.37	1.02
26	0.158	1.9	0.79	0.41	4.83
27	0.159	1.4	0.99	0.71	8.05
28	0.181	1.0	1.00	0.98	1.70
29	0.181	1.0	1.00	1.05	2.27
30	0.181	0.8	1.00	1.32	5.94
31	0.181	2.0	0.76	0.37	5.04
32	0.181	1.5	0.97	0.64	8.61
33	0.182	1.3	1.00	0.79	7.60
34	0.181	1.7	0.88	0.51	1.35
35	0.181	1.8	0.83	0.45	5.60
36	0.181	1.4	1.00	0.73	8.03

These simply excited gravity waves were approximately sinusoidal in nature. The time series from regimes 2, 18, and 35 are shown in Figure 4. Recordings were started when the first strong wave reached the measurement location, and were cropped to 6 seconds to avoid including any reflections from the flume end. Zero on the vertical axis represents the mean surface position. Note the change in scale on the vertical axis.

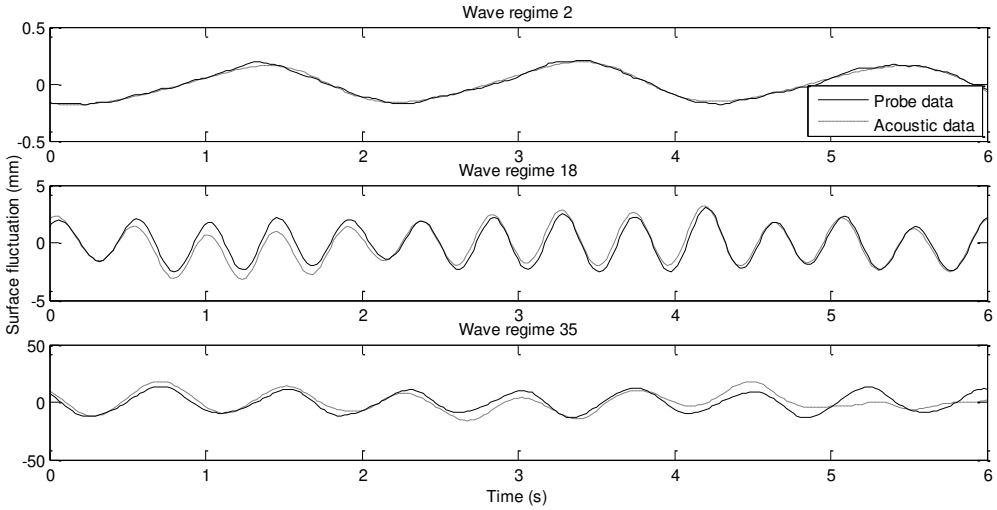

Figure 4: Comparison of acoustic and wave probe data for gravity wave time series for regimes 2, 18 and 35, with wave properties respectively: λ=1.07, 0.54, 0.45m; h_{rms}=0.11, 1.88, 5.60mm; C_p=0.88, 0.86, 0.83m/s; f=0.8, 1.6, 1.8Hz.

It can be seen that the variation in acoustic phase generally tracks the fluctuations in local water surface elevation. The system is effectively acting as an acoustic wave probe. This relationship is strong for regime 2, even though the fluctuations themselves are very small (h_{rms} = 0.11mm). For regime 18 some deviation between probe and acoustic data is observed in some areas of the time series. For regime 35 there are deviations of significant magnitude, and toward the end of the series there is sustained deviation. There are two initial explanations for this progressive error. Firstly, the Fresnel zone approximation would suggest that as the wavelength of gravity waves is decreased, errors become more likely, as closer adjacent wave features begin to affect the reflection of sound from the dominant Fresnel zone (for the experimental setup used in this work, this equates to an area with a diameter of approximately 0.11m). Secondly, as is apparent from the vertical axes in Figure 4, an increased wave height may cause an increase in the error. In order to investigate this, the measurement error was calculated for each wave regime. By comparing the wave probe data against the acoustically estimated surface elevation data it was possible to determine the mean absolute error. Since the accuracy is governed by the resolution of the phase measurement, which itself is governed by the wavelength of the acoustic signal, in order to examine the accuracy of the method the absolute error value may also be expressed as a percentage of the acoustic wavelength (7.6mm). These data are given in Table 2.

Table 2: Gravity wave measurement accuracy

Wave regime	Mean absolute error (mm)	Mean error as % of acoustic wavelength (%)	Mean error as % of 4 x RMS wave height (%)	Wavelength λ (m)	RMS wave height h_{rms} (mm)
1	0.01	0.11	5.65	0.85	0.04
2	0.01	0.13	2.36	1.07	0.11
3	0.01	0.15	1.40	1.22	0.21
4	0.01	0.10	10.90	0.51	0.02
5	0.01	0.12	4.60	0.71	0.05
6	0.01	0.17	2.12	0.77	0.15
7	0.01	0.11	12.41	0.36	0.02
8	0.01	0.12	8.94	0.56	0.03
9	0.01	0.13	3.26	0.78	0.08
10	0.02	0.31	1.31	0.94	0.47
11	0.02	0.31	0.63	1.34	0.98
12	0.05	0.58	0.94	1.13	1.23
13	0.05	0.57	2.03	0.65	0.56
14	0.07	0.91	1.72	0.82	1.04
15	0.06	0.76	0.73	1.08	2.06
16	0.04	0.56	3.09	0.31	0.36
17	0.43	5.39	6.34	0.38	1.68
18	0.22	2.75	2.89	0.54	1.88
19	0.05	0.67	0.65	1.00	2.04
20	0.35	4.44	2.43	1.36	3.60
21	0.12	1.47	0.72	1.09	4.06
22	2.38	30.12	13.00	0.38	4.58
23	3.15	39.82	12.69	0.61	6.20
24	5.73	72.52	14.67	0.77	9.78
25	0.42	5.35	10.38	0.37	1.02
26	2.71	34.25	14.02	0.41	4.83
27	5.01	63.39	15.57	0.71	8.05
28	0.07	0.89	1.03	0.98	1.70
29	0.10	1.21	1.05	1.05	2.27
30	0.35	4.48	1.49	1.32	5.94
31	3.39	42.92	16.84	0.37	5.04
32	5.37	67.87	15.59	0.64	8.61
33	3.98	50.33	13.09	0.79	7.60
34	0.11	1.33	1.95	0.51	1.35
35	3.10	39.19	13.84	0.45	5.60
36	5.45	68.94	16.98	0.73	8.03

Examining the theory that reduced wavelength or increased wave height may prompt an increase in error, the mean absolute error values are plotted against wavelength and RMS wave height in Figure 5. It can be seen that the data falls into two groups, one with low error (mean absolute error <5.4%) and one with high error (mean absolute error >30%). Although there is a general pattern among the high error data whereby decreased wavelengths and increased wave heights appear to cause increased error, this dependence cannot be relied upon because several of the low error data points have small wavelengths, and several have large wave heights.

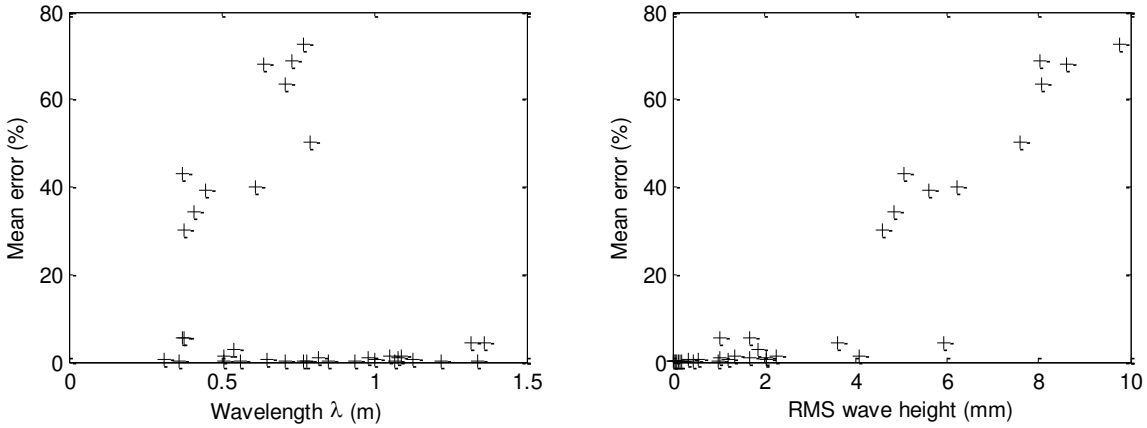

Figure 5: Mean absolute measurement error vs. wavelength and wave height

It was noted that the wavelength and wave height may be affecting the validity of the measurement technique when their influence is examined in combination. It was found that the ratio of wave height to wavelength is strongly correlated with the measurement error. Figure 6 shows the mean error as a function of the ratio of RMS wave height to wavelength.

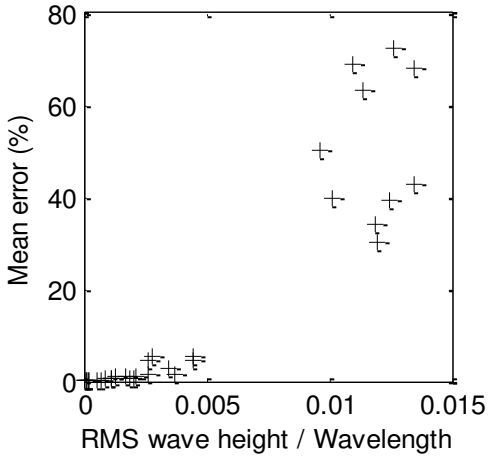

Figure 6: Mean absolute error vs. wave height / wavelength

Figure 6 can be used to define a threshold beyond which the error becomes significant. In order to guarantee that the mean error in the water elevation measurement is below 10% this threshold should be set as $h_{rms}/\lambda = 0.005$. Below this threshold the errors may be attributed mainly to the accuracy in the phase measurements. This ratio of wave height to wave length can be thought of as a measure of the local surface gradient. Indeed, by using the recorded time series, and the calculated values of Cp, the mean local gradient can be calculated for each wave regime. This is plotted against the ratio of RMS wave height to wavelength in Figure 7.

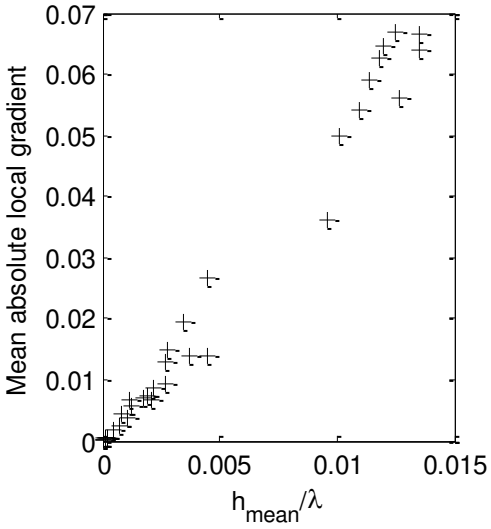

Figure 7: local gradient vs. wave height / wavelength

It can be seen that the relationship is close to linear. In this case the threshold mean absolute surface gradient beyond which the technique would likely fail is 0.025. In some applications, where the water surface pattern has a broad spatial spectrum, it may be difficult to estimate the dominant wavelength and wave height. In these instances measurements of the local surface gradients would be more practical. These results show that the validity of this measurement technique may be assessed on a site-to-site basis by visual estimation of the dominant wavelength and wave height or, for more complex surface patterns, a measurement of the local surface gradients. As the errors have been non-dimensionalised with the acoustic wavelength and expressed in terms of the local surface gradient, the result is general and provided a situation meets the wave gradient threshold the same level of accuracy can be expected.

The relative error expressed as a percentage of the wave height gives an indication of how closely the acoustic phase matches the measured wave pattern, and is a more practical description of the accuracy of the system. For wave height in this case, h_{rms} is multiplied by 4 as this represents the mean peak to trough amplitude of the waves. For the regimes which satisfy the h_{rms}/λ criterion, this relative error is plotted against $4h_{rms}$ in Figure 8.

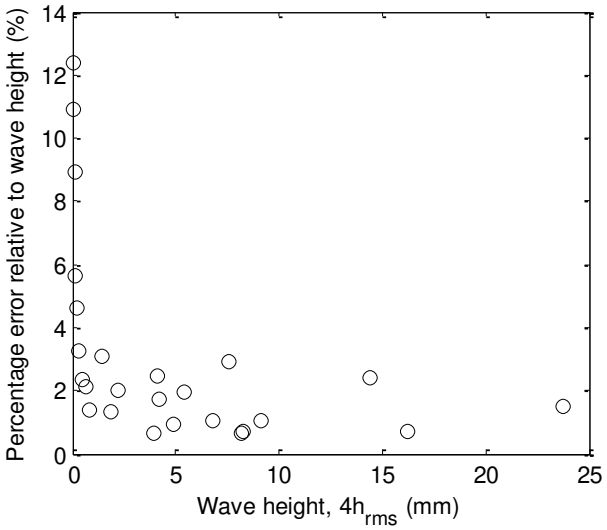

Figure 8: Error relative to wave height, *E*, plotted against wave height, $4h_{rms}$

It can be seen that as the wave height increases, the relative error, *E*, decreases. A regression through the points shows that this relative error may be expressed as a function of the wave height:

$$E \propto \frac{1}{\sqrt{h_{rms}}} \tag{9}$$

This confirms that for very small wave heights, the relative error may be large. In these experiments, for the wave regimes which satisfy the gradient criterion, the relative error becomes larger (>4%) when the RMS wave height is below 0.08mm or 1% of the acoustic wavelength. This provides an additional criterion and suggests that the wavelength of the acoustic system can be tuned to provide high accuracy for a given range of water wave amplitudes.

5. TURBULENCE GENERATED SURFACE WAVES

With the accuracy of the system quantified and validated, it was then tested on more realistic surface wave patterns. For this purpose a steady, uniform water flow over a flat gravel bed was created in the flume. These flow resulted in complex turbulence-generated water surface patterns, which were measured using the same wave probe and acoustic setup as described in section 3. The flume gradient was set to 0.004 and a range of steady flow regimes were examined. The mean flow depth and RMS wave height were calculated from the wave probe data. For this type of flow the surface features are turbulence driven rather than gravity waves, and thereby propagate at the velocity of the flow, so local surface gradients were calculated using the mean velocity and the wave probe time series. These data are presented in Table 3.

Table 3: Hydraulic flow conditions

Flow regime	Depth d (mm)	Mean velocity V (m/s)	RMS wave height h_{rms} (mm)	Mean absolute local gradient (-)
1	32	0.33	0.28	0.004
2	38	0.36	0.28	0.005
3	58	0.44	0.41	0.006
4	64	0.46	0.44	0.007
5	75	0.52	0.60	0.006
6	89	0.57	0.59	0.007
7	107	0.67	0.63	0.005
8	119	0.82	0.51	0.005

For these flow regimes the surface pattern is more complex than for gravity wave regimes, containing a broader range of frequency components. Frequency spectra for regimes 1, 4 and 7 are shown in Figure 9.

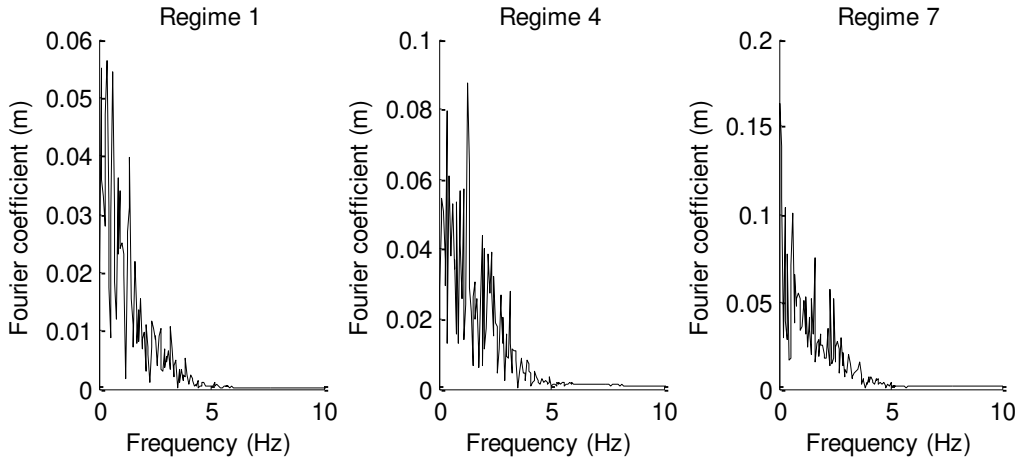

Figure 9: Frequency spectra of turbulence generated surface waves

The spectral content of the regimes is similar, albeit at different magnitudes. It can be seen that the dominant spectral components fall below around 3Hz, but the spectrum extends further in frequency up to around 5Hz. Even at the lowest velocity (regime 1, 0.33m/s), the dominant components (<3Hz) would provide a wavelength of 0.11m, just about to satisfy criterion 1. Although the components between 3Hz and 5Hz are small, they may be significant enough to violate the first criterion, particularly for regimes 1-3. Table 3 also shows that the mean local surface gradient does not exceed the predetermined limit of 0.025 (criterion 2) and that the wave heights are all greater than 1% of the acoustic wavelength (criterion 3). This would suggest that the mean absolute error should not exceed 5.4% of the acoustic wavelength, and the mean relative error should not exceed 4% of the maximum wave height ($4h_{rms}$). The results from regimes 1, 4 and 7 (see Table 3) are shown in Figure 10. It can be seen that the magnitudes of the error is similar in each case. The mean absolute error is calculated in Table 4, and is also presented as a percentage of the acoustic wavelength, and as a percentage of four times the RMS wave height, which is an estimate of the typically largest wave heights – i.e. the practical range of the water surface measurements.

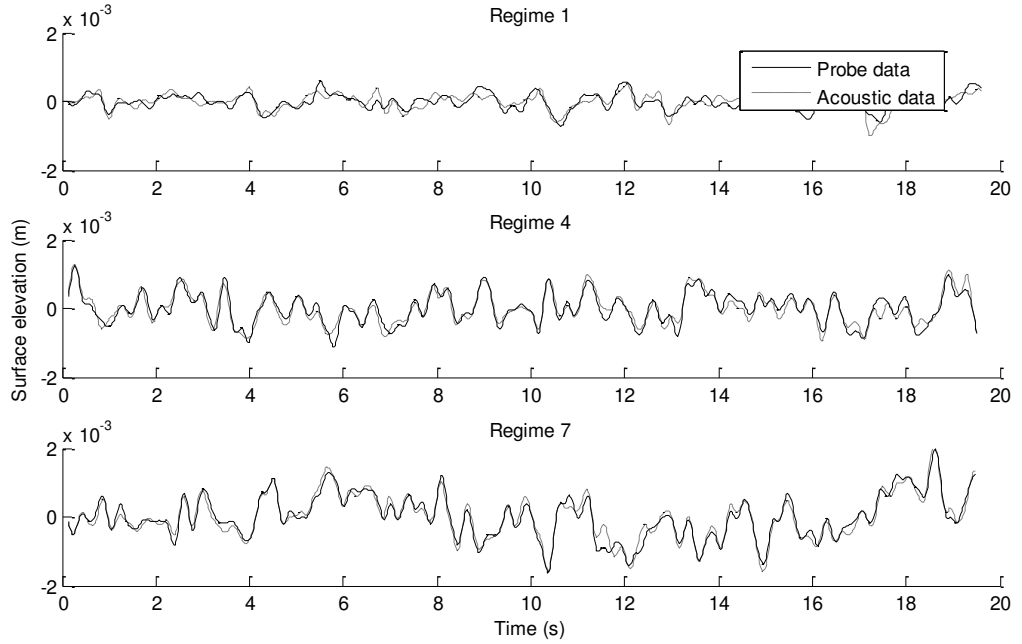

Figure 10: Acoustic wave probe accuracy for turbulent flow surface for regimes 1, 4 and 7, with flow properties respectively: d=32, 64, 107mm; V=0.33, 0.46, 0.67m/s; h_{rms}=0.28, 0.44, 0.63mm.

Table 4: Error in turbulent free surface measurement

Flow regime	RMS wave height h_{rms} (mm)	Mean absolute error (mm)	Mean error as % of acoustic wavelength (%)	Mean error as % of 4 x RMS wave height (%)
1	0.28	0.12	0.02	13
2	0.28	0.08	0.02	16
3	0.41	0.11	0.02	10
4	0.44	0.08	0.02	7
5	0.60	0.05	0.01	5
6	0.59	0.13	0.02	8
7	0.63	0.08	0.02	5
8	0.51	0.09	0.02	8

The absolute error is reasonably low and reasonably constant and does not appear to be a function of the local gradient (perhaps because the gradients are so far below the limits defined in section 4). Errors here are most likely due to incoherent acoustic scattering as some of the surface wavelengths violate the Fresnel zone limit of the first criterion, and also due to inherent inaccuracies in the phase measurement governed by the initial sample rate, and the accuracy of the data acquisition and phase detection systems. In flow regimes with smaller wave heights these absolute errors cause greater relative deviation between the wave probe and acoustic data (as can be seen from regime 1 in Figure 10). For regimes which strongly violate criterion 1 (regimes 1-3), the error relative to the wave height is above 10%, but for the other regimes the relative error is more acceptable at less than 10%. This is approximately twice the relative error measured for gravity waves, and is most likely due to the more complex nature of the turbulence generated waves (i.e. small wavelength components causing some amount of interference of the acoustic signal). This could be improved further by optimising the acoustic wavelength if small water wave heights are to be measured, and adjusting the geometry of the acoustic equipment in order to minimise the first Fresnel zone.

6. CONCLUSIONS

It has been shown that for several free surface wave regimes, analysis of the temporal variation of the phase difference between a sent and received signal reflected from the dynamically rough surface facilitates direct non-invasive measurement of the surface elevation over time at a small point on the surface. Effectively the equipment behaves as an acoustic wave probe, and this is validated by comparison with data from a standard conductance based wave probe.

A theoretical minimum wavelength is determined based on established theory of Fresnel zone ensonification (criterion 1). The dominant wavelengths examined in this work have been greater than this limit. Using artificially generated gravity waves it was determined that the magnitude of the local surface gradient could significantly affect the validity of the acoustic approach. This may be through a combination of effects. Firstly, a significant local gradient at the point of specular reflection would cause the majority of the acoustic energy from that point to be reflected in a direction other than that of the receiver, yielding low signal levels from the point of interest. Secondly, high gradients may give rise to multiple scattering effects, whereby an acoustic path may make contact with two or more points on the flow surface before reaching the receiver, obscuring any useful phase information. Using this information a surface gradient limit is defined beyond which the technique is liable to give erroneous readings (criterion 2). Finally the errors were examined in relation to the scale of water waves under investigation, and it was found that the relative error increased significantly as the RMS wave height became very small, leading to a wave height limit in terms of the acoustic wavelength (criterion 3).

Using these established criteria, turbulence generated water surface waves were examined. It was found that the surface waves on all the flow regimes satisfied the three established criteria. This

resulted in mean absolute errors being below 0.02% of the acoustic wavelength, and mean relative errors below 10% of the representative wave height.

However, these errors may be reduced further. The presented technique for liquid surface fluctuation monitoring can be tuned to the fluctuations of interest by selecting an acoustic frequency to ensure that the acoustic wavelength is suitable for the water wave heights, and by optimising the component geometry such that the operative Fresnel zone is smaller than the dominant wavelengths.

This technique provides a unique, low-cost non-contact method for quantifying fluid surface fluctuations. Such a device would enable robust and efficient monitoring of surface properties in a number of applications, and coupled with the findings of Horoshenkov et al (2013), may even be used to monitor the hydraulic properties of shallow flows. While an acoustic approach is sensible for local measurements, the technique is also suitable for alternative excitation signals, such as microwaves, or radio frequency signals. These techniques may be more robust to changes in atmospheric conditions, and may be operated over a greater distance.

7. ACKNOWLEDGMENTS

This work was conducted with funding provided by Yorkshire Water Services and the UK's Engineering and Physical Sciences Research Council (Grant EP/G015341/1).

8. REFERENCES

Nichols, A., Horoshenkov, K., Shepherd, S., Attenborough, K. and Tait, S. (2010), *Sonic characterisation of water surface waves,* Advances in Hydraulic Physical Modelling and Field Investigation Technology, pp 40-47.

Denissenko, P., Lukaschuk, S., and Nazarenko, S., *Gravity surface wave turbulence in a laboratory flume,* Physical Review Letter 99 (1).

Wilde, P., Szmidt, K., and Sobierajski, E. (1998), *Phenomena in standing wave impact on a horizontal plate*, Coastal engineering, Vol. 2, pp 1489-1501.

Bullocka, G., Obhraia, C., Peregrineb, D., Bredmoseb, H. (2007), *Violent breaking wave impacts. Part 1: Results from large-scale regular wave tests on vertical and sloping walls*, Coastal Engineering, Vol. 54 (8), pp 602–617.

Barjenbruch, U., Mai, S., Ohle, N., Mertinatis, P. And Irschik, K. (2002), *Monitoring of water level, waves and ice with radar gauges,* Proceedings of Hydro 2002, Kiel, Germany.

Daida, J., *Measuring topography of small-scale water surface waves,* Proceedings of the 1995 International Geoscience and Remote Sensing Symposium: Quantitative Remote Sensing for Science and Applications.

Takamasa, T. and Hazuku, T. (2000), *Measuring interfacial waves on film flowing down a vertical plate wall in the entry region using laser focus displacement meters*, Int. J. Heat Mass Transfer 43, pp. 2807-2819.

Tsubaki, R. And Fujita, I. (2005), *Stereoscopic measurement of a fluctuating free surface with discontinuities,* Meas. Sci. Technol. 16, pp 1894-1902.

Lagergren, P. (2012), *Ultrasonic fuel level monitoring device,* US patent 7287425.

Redding, R. (1983), *Measurement of distance using ultrasound,* UK patent GB2121174A.

Wang, Y., Mingotaud, C., amd Patterson, L. (1991), *Noncontact monitoring of liquid surface level with a precision of 10 micrometers: A simple ultrasound device,* Rev. Sci. Instr. 62 (6), pp 1640-1641.

Delafon, P. (1973), *Method and devices for measurement of position,* French patent 73 29663.

Oelze, M., Sabatier J. and Raspet, R. (2003), *Roughness Measurements of Soil Surfaces by Acoustic Backscatter,* Soil Sci. Soc. Am. J. 67, pp 241-250

Attenborough, K. and Taherzadeh, S. (1995), *Propogation from a Point Source over a Finite Impedance Boundary*, J. Acoust. Soc. Am. 98, pp 1717-1722.

Nichols, A., Attenborough, K. and Taherzadeh, S. (2011). *Deduction of static surface roughness from complex excess attenuation*, Journal of the Acoustical Society of America, 129 (3), EL89-EL93.

Tolstoy, I. (1984) *Smoothed Boundary Conditions, Coherent Low Frequency Scatter, and Boundary Modes*, J. Acoust. Soc. Am. 75, pp 1-22.

Cooper, J., Tait, S. and Horoshenkov, K. (2006), *Determining Hydraulic Resistance in Gravel-bed Rivers from the Dynamics of their Water Surfaces*, Earth Surface Processes and Landforms, John Wiley & Sons, Ltd.

Nocke, C. (2000), *In-situ acoustic impedance measurement using a free-field transfer function method*, Applied Acoustics 59, pp 253-264.

Spandöck, F. (1934), *Experimental investigation of the acoustic properties of materials through the Kurzton method,* Ann. d. Phys .Vol 412 (3), pp. 328–344.

Airy, G. (1841), *Tides and waves,* In Hugh James Rose, et al., *Encyclopaedia Metropolitana*, Mixed Sciences 3, pp 1817–1845.